PCCP

Wired for Stability: Evaluating Electrical Performance in Zinc Oxide-Modified Silver Nanowire Solution-Processed Transparent Electrode

Journal:	*Physical Chemistry Chemical Physics*
Manuscript ID	CP-ART-08-2024-003141.R1
Article Type:	Paper
Date Submitted by the Author:	25-Sep-2024
Complete List of Authors:	Lukic, Jovan; University of Belgrade Faculty of Technology and Metallurgy, Radmilović, Vuk; University of Belgrade Faculty of Technology and Metallurgy

COMMUNICATION

Wired for Stability: Evaluating Electrical Performance in Zinc Oxide-Modified Silver Nanowire Solution-Processed Transparent Electrode

Received 00th January 20xx,
Accepted 00th January 20xx

DOI: 10.1039/x0xx00000x

Jovan N. Lukic,[a] and Vuk V. Radmilović [a*]

Silver nanowires (AgNW) have gained much attention due to their optoelectronic and mechanical properties and are therefore potential candidates to tackle intrinsic drawbacks of currently applied transparent electrodes in various (opto)electronic devices. In order for AgNW to be justifiably considered as viable it is necessary to address their insufficient stability by coupling them with another constituent into a nanocomposite. For this purpose, ZnO has been chosen due to its low cost, solution processability and barrier properties. In this paper, a fully solution processed AgNW/ZnO TE film was investigated in order to understand the effect of ZnO coating on the electrical stability of AgNW including the mechanism of degradation during exposure to high electrical current densities. The nanocomposite transparent electrode was processed with ZnO coatings as to determine its effect on optoelectronic properties and electrical stability, where the ZnO triple coated AgNW demonstrated the best combination of optoelectronic properties and stability at highest working voltage.

Introduction

With the ever-rising demand for high-performance heterostructured (opto)electronic devices, so far there have been two approaches for improving their various properties. One approach deals with designing novel devices utilizing new technologies and materials, while the other deals with improving properties of individual components which comprise the heterostructure, having in mind their compatibility, especially at appropriate interfaces. In multilayered optoelectronic devices such as solar cells, organic light emitting diodes, transparent heaters and smart windows, transparent electrodes (TE) are components (layers) that significantly contribute to overall performance of the device, through increased light transmission, charge carrier collection and transfer while providing a distributed electrical field [1]. The most successfully applied TE has been indium tin oxide (ITO) due to its high transmittance, low sheet resistance and excellent stability [2], albeit with certain drawbacks that hinder its sustainable application, such as the ever growing cost of indium, demanding processing methods and the inability to transmit in the UV/IR part of the electromagnetic spectrum, to name a few [3]. Metallic nanowires, exhibiting high optical transmittance, high mechanical flexibility and low electrical sheet resistance, could pave the way as suitable replacements for ITO [4]. Having the option of being solution processed at relatively low temperatures, these nanowires are a class of materials which have the potential for high marketability.

Among these quasi-one-dimensional nanostructures used, silver nanowires (AgNW) offer a compelling advantage owing to their electrical conductivity, superior stability to oxidation compared to copper nanowires as well as their cost-effectiveness relative to gold nanowires [4,5]. Nevertheless, AgNWs along with other metal nanowires possess drawbacks in certain TE criteria such as low adhesion, high surface roughness and insufficient chemical, thermal, mechanical or electrical stability [4,6], which is detrimental to long term performance, and thus, foreseeable commercialization. These disadvantages can be tackled by optimizing AgNW morphology through variation of synthesis parameters or by modifying the surface through the nanocomposite approach thereby improving optoelectronic and/or mechanical properties. During synthesis of AgNW, polyvinylpyrrolidone (PVP) polymer coating induces the growth of (111) planes of Ag, but unfortunately increases the junction resistance between AgNW in contact, as does small contact area between connecting nanowires. This has been elucidated by measuring the conductivity of a single AgNW and the point where two AgNW connect, where the resistance is higher by one order of magnitude [7]. A simple yet effective way to decrease the resistance is by welding the junctions by applying a source of external energy such as thermal annealing [8], light induced welding [9], mechanically induced welding [10] and capillary force induced welding [11]. Another approach for reducing

[a] Faculty of Technology and Metallurgy, University of Belgrade, Serbia.
† Electronic Supplementary Information (ESI) available at DOI: 10.1039/x0xx00000x

junction resistance for AgNW is to apply a coating to fill in the gaps on the substrate between the nanowires i.e. forming a nanocomposite [12,13], which allows for additional conductive pathways for incoming charge, with metal oxides such as TiO_2, SnO_2, $Al2O_3$ and ZnO [13–18]. The latter, zinc oxide (ZnO) is a widely used, inexpensive, metal oxide that is solution processable and an n-type semiconductor with high electron mobility [19–21]. Additionally, synthesis through sol-gel and precipitation methods and simple solution-processing give rise to ZnO nanoparticle (NP) utilization for a cost-effective improvement of AgNW stability. So far there has been work regarding the AgNW/ZnO system in various applications such as flexible organic solar cells [22–25], transparent heaters [26] and UV photodetectors [27]. Recently, it has been reported that ZnO, a diffusion protective layer for AgNW, would delay the effect of spheroidization thus improving thermal stability of AgNW [20]. Finally, it is required to anneal the film to form a more uniform coating as well as to remove any excess solvent, which in the case of ZnO is performed at low temperatures, a favourable processing step due to lower energy consumption during processing.

Nanocomposite AgNW/ZnO films have been processed through various techniques including spray coating [28–30], atomic layer deposition (ALD) [20,31], sputtering [32] and spin coating [33,34]. While sputtering and ALD are advantageous through precise control of the thickness of ZnO on the AgNW network, spin coating, on the other side, provides a simpler, scalable and cost-effective processing route without the use of demanding and energy consumptive conditions [35]. Addressing electrical stability of fully solution processed AgNW/ZnO is essential for understanding the long-term behaviour of these cost-effective TE. Other than having sufficient concentration of AgNW to remove localized hotspots [36], it has been stated that spin coated AgNW networks form a non-homogenous electrical field at the macroscale, due to the orientation of AgNW during deposition [37]. A way of overcoming this could be through coating with ZnO NPs where the sheet resistance of the AgNW network decreases as gaps between the nanowires are filled with the nanoparticles, thus creating new pathways for charge carriers, all the while keeping a high optical transmittance of the film. Additionally, AgNW/ZnO nanocomposites have low junction resistance, thus forming an ohmic contact between the constituents and allowing for potential use as a TE in optoelectronic devices [33]. So far, AgNW/ZnO nanocomposites processed by ALD or sputtering have been analysed to determine electrical, thermal and chemical stability of AgNW and the effect that ZnO has on AgNW networks [20,26]. Nevertheless, this material combination has not yet been thoroughly analysed regarding electrical stability, in the case of solution-processed via spin coating, where precise control of coating uniformity of ZnO presents a challenge.

In this work, a fully solution processed TE based on AgNW/ZnO nanocomposite has been presented, for its ease of processing, scalability potential, and cost-effectiveness compared to ALD/sputtering techniques reported in the literature, in order to analyse the effect of ZnO NP coating on the electrical stability of AgNW, demonstrated through various voltage ramp measurements. Morphology of samples and optoelectronic properties such as transmittance and sheet resistance were also analysed before and after degradation to acquire insight into the benefits of ZnO addition to AgNW performance.

Experimental

Materials

AgNW (Sigma Aldrich) with diameter 115nm and length 20-50µm; isopropyl alcohol IPA (ZorkaPharm, Serbia), zinc acetate dihydrate ($Zn(Ac)_2$), sodium hydroxide (NaOH) and methanol (Centrohem, MOSS, HeMOSS and ZorkaPharm, Serbia respectively).

Formation of AgNW/ZnO transparent electrodes

Transparent electrodes (TE) were deposited using spin coating at various speeds and concentrations of AgNW/IPA dispersions as to determine the optimal transmittance/sheet resistance and the concentration of the percolation threshold. AgNW/IPA dispersion with a ratio of 1:1 was coated at 1000 rpm for 30s on previously cleaned glass substrates of 2.5 x 2.5 cm^2 surface area, after which it was thermally annealed for 15 minutes at 230°C to induce welding at AgNW junctions i.e., between AgNW in contact. Subsequently, ZnO NPs/DI water dispersion (ZnO NPs were synthesized through a modified sol-gel approach according to Sun et al. [38]) was coated at 2000 rpm on top of AgNW. The number of coating ZnO layers 1 (AgNW/1x ZnO), 2 (AgNW/2x ZnO) and 3 (AgNW/3x ZnO), with the system being annealed after each ZnO deposition at 140°C for 1h to ensure the removal of any excess solvent.

Synthesis of ZnO nanoparticle solution

The solution was heated to 60°C with constant magnetic stirring. In another flask NaOH (0.364 g, 9.1 mmol) was dissolved in 30ml of methanol also stirred at 60 °C and added slowly over a period of 30 minutes to the $Zn(Ac)_2$ solution. After the full volume of the NaOH solution was added, the solution of $Zn(Ac)_2$ was stirred additionally for 2 h and 15 min and subsequently centrifuged at 6000 rpm for 10 min to separate the supernatant from the formed gel. Following centrifugation, the left-over gel was washed multiple times with deionized water, ethanol and acetone. The washed gel was dried at 140 °C for 8 h, after which the resulting ZnO was ground to a fine powder using a mortar and pestle. To prepare the dispersion of ZnO NPs the ultrasonic probe from Sonics Vibra cell with the power of 750 watts and 20 kHz processor, where the amplitude of the probe was 70 %. The ZnO NPs dispersion were synthesized by adding ZnO fine grounded powder into DI at a concentration of 10 mg/ml where the solution was stirred for 1 hour and subsequently ultra-sonicated for 2 h to achieve stability.

Characterization methods

Scanning electron micrographs were obtained by FESEM Tescan Mira3. Transmission electron microscopy (TEM) of ZnO NPs was performed on a Thermofisher Talos F200X G2 while scanning transmission electron microscopy (STEM) along with energy

dispersive X-ray spectroscopy analysis (EDX) was performed on Thermo Fisher TitanX 60-300 for the lamella sample prepared on a Thermo Fisher Scientific Helios G4 CX DualBeam SEM/FIB system. X-ray diffraction (XRD) was performed on Ultima IV Rigaku diffractometer equipped with Cu Kα radiation, 2θ range of 10 ° - 90 °, continuous scan mode with a scanning step size of 0.02 ° and scan rate of 2 °/min. The optical transmittance of welded, coated and degraded samples, was analysed using a Shimadzu 2400 UV-Vis spectrophotometer, equipped with an integrating sphere. Electrical sheet resistance was performed using a four-point probe in combination with a Keithley 2000 source meter. Three types of measurements have been performed to analyse the electrical stability of AgNW/ZnO electrodes a) voltage ramp at a constant 0.6 V/min for inducing degradation through resistance divergence, b) cyclic voltage ramp, 4 V – 10 V, for analysing stability under dynamic electrical stress, c) voltage plateau measurements, giving insight into behaviour under constant high voltage ramps, with 2V steps (15min each) ranging from 1 V to 7 V and back to 1 V. The first two measurements were performed on a two probe Keithley 2400 source meter setup while the third was done on a Gamry Interface 1010E potentiostat using chronoamperometry measurements.

Detailed information of AgNW/ZnO formulation can be found in the ESI.

Results and discussion

Synthesized ZnO NP powder is depicted in Figure 1a with particle size calculated to be in the 29.06 ± 11.78 nm range (Figure 1b).

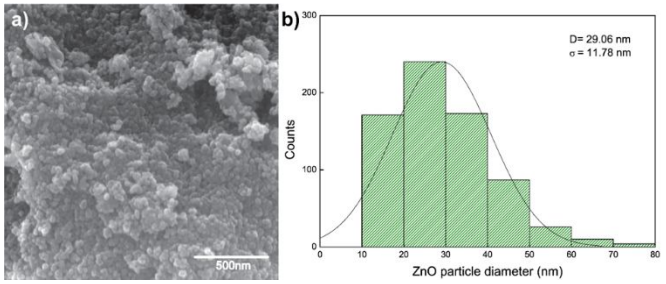

Figure 1. a) synthesized ZnO NP powder, b) histogram of size distribution of ZnO NP based on SEM micrographs.

The XRD pattern (Figure 2a) of synthesized ZnO NP is in very good agreement with JCPDS card no. 01-089-1397, indexing hexagonal wurtzite ZnO phase having the P63mc (186) space group, a = 3.2494 Å, c = 5.2054 Å, indicating pure phase ZnO. Slight peak broadening indicates the formation of nanocrystals in the samples [39]. Eleven diffraction peaks (100, 002, 101, 102, 110, 103, 200, 112, 201, 004 and 202) are present in the diffractogram, which are represented by their respective Miller indices and thus show (Figure 2a) good crystallinity of the sample.

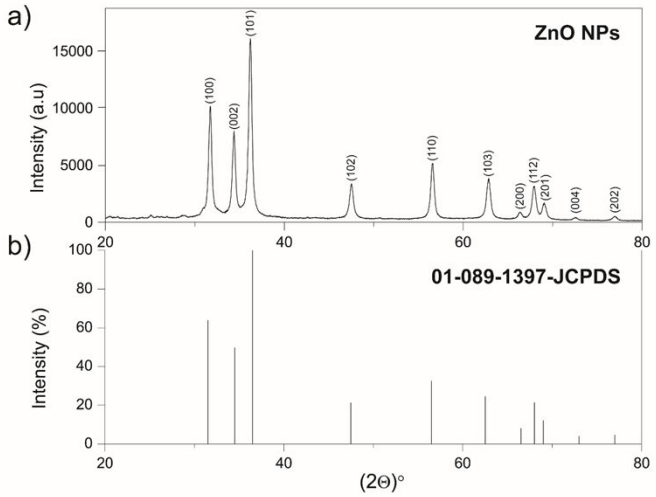

Figure 2. a) XRD pattern of the synthesized ZnO NP powder and b) the corresponding JCPDS card showing the 2θ peak positions.

Figure 3a depicts a TEM image of a typical ZnO nanoparticle cluster, where particle size from similar images was calculated to be 27.34 ± 7.55 nm. Figure 3b and 3c represent an experimental selected area diffraction pattern (SAED) taken from the area noted in Figure 3a and simulated ring diffraction pattern of a perfect ZnO wurtzite structure, respectively. Figure 3d represents a line profile (intensity vs. spacing) of the experimental SAED pattern with noted reflections. The experimental ring pattern correspond to the simulated DP, with the line profile noting the intensity peaks which correspond to reflections that are in good agreement with the XRD analysis of ZnO, confirming the presence of pure ZnO wurtzite phase.

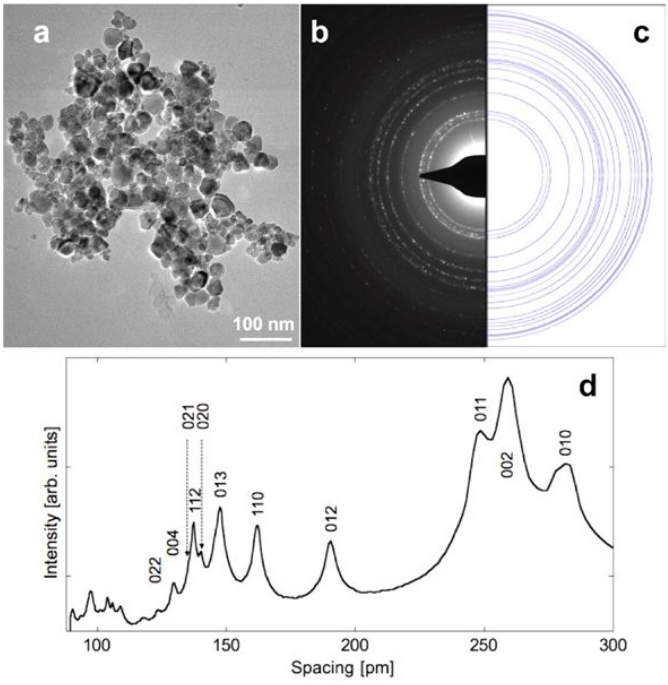

Figure 3. a) Low magnification TEM image of ZnO nanoparticles; b) SAED pattern of ZnO nanoparticles shown in TEM image a); c) simulated DP ring of ZnO wurtzite structure; d) rotational average line profile of experimental SAED with appropriate Miller indices.

The morphologies of pristine (Figure 4a) and annealed AgNW (Figure 4b) are presented in SEM images where it is clear that the heat treatment induced solid state wetting and welding of nanowire junctions. There is an expected trend of rising surface coverage of ZnO with the increase of number of ZnO coatings i.e. from one i.e. AgNW/1x ZnO (Figure 4c), where uncoated surfaces are more than evident than in the case of triple coated AgNW i.e. AgNW/3x ZnO (Figure 4d).

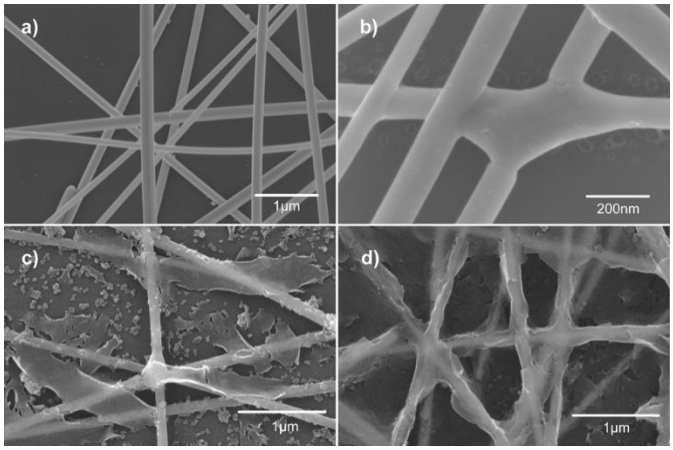

Figure 4. a) SEM image of pristine spin coated AgNW; b) SEM image of a welded junction of AgNW after annealing; welded AgNW coated c) once with ZnO NPs, AgNW/1x ZnO, and d) three times with ZnO NPs, AgNW/3x ZnO.

As a way of elucidating the intimate contact between welded AgNW (henceforth referred to as only "AgNW") and ZnO, the cross section for the AgNW/3x ZnO analysed (Figure 5) via STEM along with EDX in order to acquire elemental distribution within the sample. Typical five-fold symmetry of the AgNW can be seen, where the five twin segments of the AgNW are divided by twin planes. EDS mapping of Ag (red), Zn (blue) and O (yellow) demonstrates the presence of all elements in appropriate phase where ZnO nanoparticles form the shell around the AgNW. The topology of the presented phase suggests that ZnO shell could act as a barrier layer [20].

With the addition of ZnO layers, the surface roughness decreased in value (Fig. S2a) from 303 nm for welded AgNWs to 208.49 nm with the addition of one coating of ZnO (AgNW/1xZnO), 235.61 nm for two coatings (AgNW/2xZnO) and 137.24 nm for the triple coated AgNW TE (AgNW/3xZnO). The decrease of surface roughness of TE is beneficial for overall efficiency of any optoelectronic device as it leads to reduction of light scattering, short circuiting and increase of electrical conductivity through better layer contact.

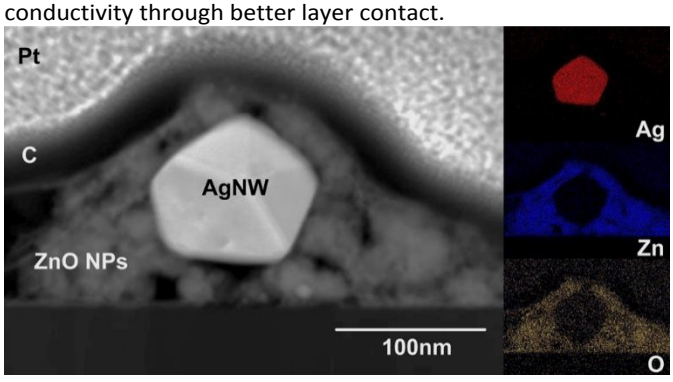

Figure 5. STEM image of AgNW/3x ZnO cross section with appropriate EDX maps depicting elemental distribution of Ag, Zn and O where the Pt and C indicate the platinum and carbon protective layers deposited during sample preparation.

Results of optical transmittance measurements (at 550 nm wavelength), one of the key properties for transparent electrodes, are given in Figure 6 (full transmission spectra given in Fig. S3a), as a function of number of coated ZnO layers as well as sheet resistance, prior and subsequent to static/dynamic electrical stress. While AgNW/1x ZnO exhibited transmittance of 88.2 %, comparable to pristine AgNW, increasing the number of ZnO layers leads to a drop in transmittance for AgNW/2x ZnO and AgNW/3x ZnO, 84.69 % and 82.17 % respectively (Figure 6a). Following the electrical stress measurements, the samples were analysed again to elucidate the possible effect on the optical properties. A drop in transmittance was expected likely due to the oxidation of silver through heating by electrical current during degradation (Fig. S3b) which can be corroborated by the lack of the surface plasmon peak [40,41] at ~360 nm, mostly noted for the AgNW and AgNW/1x ZnO samples.

Annealing of AgNWs and hence welding of junctions reduced their electrical sheet resistance (R_S) from 74.2 to 23.2 Ω/□ with a negligible difference in transmittance. With the addition of the first layer of ZnO, R_S increased to 31.4 Ω/□ which can be attributed to the high resistance of ZnO NP, while the transmittance remained approximately the same (88.2 %). After the second layer of ZnO, R_S dropped down to 20.7 Ω/□ with the transmittance of 84.6 % which can be possibly attributed to ZnO NP film formation in previously empty gaps between the AgNW, which are now connected with a bridge of ZnO thus creating additional charge pathways, while the values for AgNW/x3 ZnO were noted to be 24.6 Ω/□ for R_S and 82.16 % transmittance (Figure 6b). Higher sheet resistance of a thin ZnO layer (1xZnO) on AgNW is most likely due to increased junction resistance and insufficient passivation. In this case, Schottky barriers at AgNW junctions are formed, leaving the nanowires exposed to oxidation, which leads to resistance increase. In contrast, a thicker ZnO (2xZnO and 3xZnO) layers improve ohmic contact, protecting the AgNWs from oxidation, thus enhancing junction stability and in turn, lowering sheet resistance.

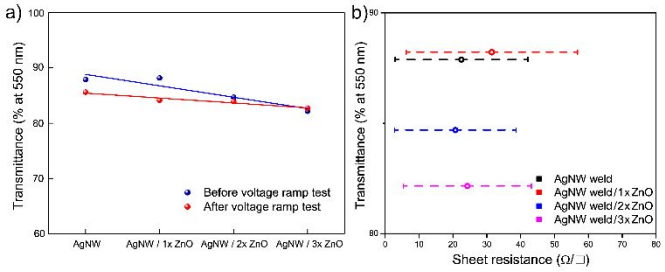

Figure 6. a) UV-VIS transmittance at 550 nm of AgNW and various AgNW/ZnO before (blue) and after (red) voltage ramp testing, b) UV-vis transmittance at 550 nm as a function of sheet resistance of AgNW and various AgNW/ZnO after voltage ramp test, with noted error bars.

The values of total transmittance at 550 nm (omitted glass substrate influence) and sheet resistance for the AgNW/3x ZnO TE were 88.36 % and 24.6 Ω/□, respectively, are comparable to

those that Khan et. al. [20] obtained using energy demanding atmospheric pressure spatial atomic layer deposition (AP-SALD) where the sheet resistance and transmittance value at 550 nm were 10 Ω/□ and ~90 %, respectively.

The difference in morphology before (Figure 7a) and after (Figure 7b) voltage ramp tests show the breakdown of junctions of two nanowires and the formation of voids and spheres on the surface of the AgNW. This change can be the result of a synergistic degradation effect caused by both electromigration, due to a short range DC stress, and spheroidization, caused by the Joule heating of the network [42]. Electromigration, as an AgNW failure mechanism, is caused by the momentum transfer between Ag atom nuclei and electrons under high current density. With this in mind, it is highly likely that AgNW junctions degrade first (Figure 7b) and thus instigate the degradation of the whole network [43]. When an electric current passes through a conductive network, the current flows simultaneously through all channels where, depending on the resistance of each pathway, various densities of current will be achieved [44]. As proposed by Koo et al. [43] AgNW networks conduct current through a primary path. The amount of current passing through a path depends on the number of junctions present in that path. When the primary path starts to degrade, secondary paths start to conduct since the current favours lower resistance paths, eventually leading to failure of the AgNW network through a combined effect of Joule heating and electromigration. With this in mind, high aspect ratio AgNWs provide greater electrical stability, the reason primarily due to lower number of junctions involved in the electrical percolating network [4]. Lower stability can be ascribed to solution processing in ambient conditions as well as effects stemming from spin coating, where there is a preferential orientation of equipotential lines of potential maps which causes electrical inhomogeneity [20,37]. Thus, this work dealt with the effect of increasing the number of ZnO coatings on the AgNW electrical stability, based on failure voltage occurring with voltage ramp testing.

Values for current density of the AgNW and AgNW/3x ZnO samples have been calculated to be 0.95 x 1010 Am^{-2} and 1.75 x 1010 Am^{-2}, respectively, based on the physical model formulated by Lagrange et. al. [45]. Although this indicates the spheroidization effect taking place, based on values of current density from literature for a single crystalline AgNW, and the elucidated morphology, showing both voids and the formation of spheres, of the degraded AgNW (Figure 7b) the mechanism for degradation in this case is likely a combination of spheroidization and electromigration.

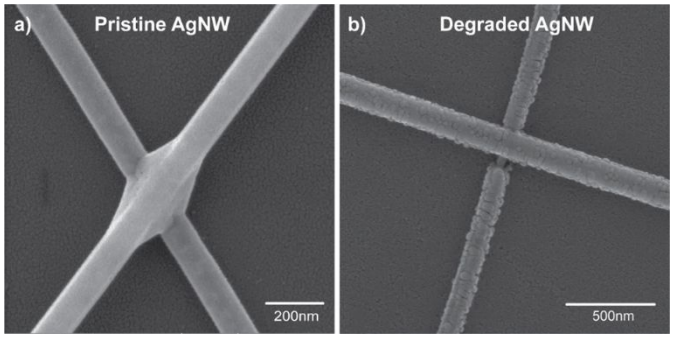

Figure 7. SEM micrographs of a) pristine welded AgNW and b) degraded AgNW affected due to the combination of electromigration and spheroidization.

Failure voltage is noted as the indication point of AgNW network breakdown under voltage ramp, which increases with each new ZnO layer (Figure 8a). The sudden increase of resistance i.e. AgNW network breakdown, occurs at 6.8 V for uncoated AgNW and with each coating of ZnO, the value increases: 9.2 V (AgNW/1x ZnO), 10.3 V (AgNW/2x ZnO) and 12.7 V (AgNW/3x ZnO). Although the AgNW/2x ZnO TE showed the most promising combination of transmittance and R_S, AgNW/3x ZnO exhibited the highest electrical stability which likely stems from the fact that there is better coverage of AgNW with ZnO for the AgNW/3x ZnO sample and thus improved barrier properties. This trend is comparable to the effect that the increase of diameter of the AgNW leads to the increase of the spheroidization temperature [46]. Since this degradation is a combined effect of electromigration and spheroidization [47], failure voltage is comparable with the spheroidization temperature according to Joule's law. With this in mind the abovementioned values of failure voltage, as a trend, are noted in Figure 8b for pure AgNW, and covered by the single ZnO (red square), double ZnO (blue square) and triple ZnO layer of nanoparticles (magenta square). The failure voltage or nanocomposite of AgNW core surrounded by triple layered nanoparticle shell is twice as large compared to the failure voltage for uncoated AgNW (6.8 V), an example of how solution processed ZnO shell could be utilized as a low-cost protective material for AgNW.

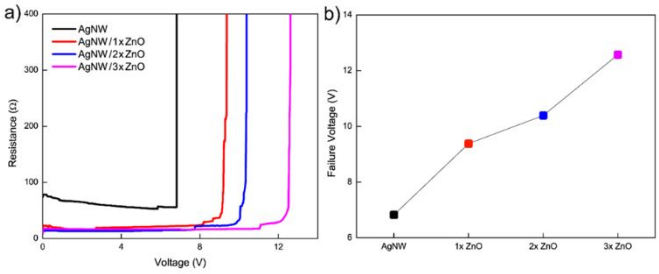

Figure 8. a) Voltage ramp of AgNW and ZnO coated samples for uncoated AgNW (black), AgNW/1x ZnO (red), AgNW/2x ZnO (blue) and AgNW/3x ZnO (magenta), b) dependence of failure voltage vs number of coatings of ZnO - uncoated AgNW (black), AgNW/1x ZnO (red), AgNW/2x ZnO (blue) and AgNW/3x ZnO (magenta).

To understand how a TE would behave in a working device, with and without bias, voltage ramp and voltage plateau measurements are essential for assessing performance [45]. As such, AgNW and AgNW/ZnO samples were subjected to cyclic voltage ramps of high electrical current (Figure 9a, for the highest voltage value, 433 mA). For AgNW (black line) degradation was present during the whole process of voltage cyclic ramps. This can be deduced from the sudden increase in relative resistance at the maximums of the voltage ramps e.g. at the 9 min and 14 min mark (maximums as markers are depicted in inset of Figure 9a for trend comparison between the two samples) which can be associated with the electron-phonon interaction [45]. The maximum values of the voltage ramp cycles represent the points where the highest temperatures in

the samples occur, due to Joule's law, these temperatures combined with high values of current lead to spheroidization and electromigration causing degradation of the AgNW which can be seen as deviation of the linear trend [14]. The resistance for the AgNW subsequently deviates from the linear maximum values which can be ascribed to the further welding of previously unwelded nanowire junctions and finally irreversible degradation. On the other hand, AgNW/3x ZnO (red line) showed no change in the linear trend of the relative change in resistance as the experiment proceeded, indicating no degradation present.

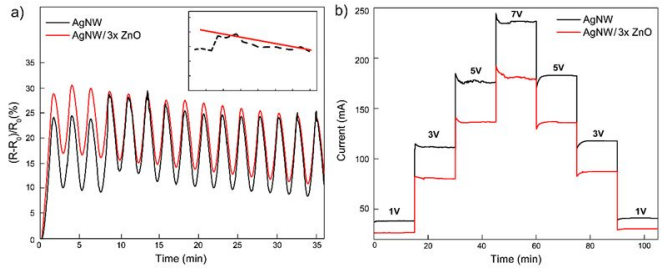

Figure 9. a) Relative change in electrical resistance of AgNW network and AgNW/3x ZnO nanocomposite versus time during voltage ramp cycles between 4V and 10V with inset depicting maximum relative change in resistance for the AgNW and AgNW/3x ZnO layer composite, where the red line indicates linear relationship, after initial perturbation; b) Voltage plateau ramp measurements for AgNW and AgNW/3x ZnO nanocomposite with noted voltage plateau values.

Aside from cyclic voltage ramps it is necessary to perform voltage plateau measurements to further assess the electrical stability of a TE. Voltage plateaus were applied at identical intervals, with a duration of 15 min each, with a total of seven steps. AgNWs (Figure 9b) exhibit degradation and instability from the 5 V plateau indicated by the current fluctuation occurring during the whole plateau. The higher the voltage plateau, larger fluctuation is present. For the AgNW/3x ZnO, degradation occurs only when hitting the later, 7 V plateau mark, which can be assigned as the beginning of irreversible degradation [20], thereby confirming a stability threshold for higher electrical current than the uncoated AgNW.

Conclusions

In order to elucidate the effect of ZnO NP deposition on AgNW performance as a transparent electrode, electrical stability, sheet resistance and optoelectronic properties were analysed. Although ZnO as an efficient barrier layer for AgNW has been reported in literature, there is generally a lack of findings regarding insights into cost-effective and scalable solution processing methods for stabilizing AgNW with ZnO. Microstructural analysis of the ZnO NP powder, obtained by XRD and TEM, confirmed the wurtzite structure of ZnO. Successive coatings of ZnO on AgNW were analysed through various electrical stability tests. Although the AgNW/2x ZnO sample had superior optoelectronic properties with 24.6 Ω/□ and total transmittance at 550 nm of 88.36 %, AgNW/3x ZnO had the highest failure voltage value of 12.7 V which was almost double to that of AgNW, 6.8 V. Barrier properties of ZnO were analysed through transmittance measurements before and after voltage ramp tests, where the values for AgNW/3x ZnO had negligible change in transmittance. Based on the idea that the ZnO coated AgNW degrade at later stages of voltage ramp measurements, the beneficial effect that the ZnO layers has on the overall electrical stability of AgNW networks can be proposed. Results obtained for ZnO NP as a solution processed protective layer for AgNWs, show promise for the application of this nanocomposite material as a transparent electrode in optoelectronic devices.

Author contributions

Jovan N. Lukić: Investigation, Methodology, Writing – Original Draft, Visualization. **Vuk V. Radmilović**: Supervision, Conceptualization, Resources, Writing – Review & Editing.

Acknowledgement

The authors thank Marko Bošković (Institute of Chemistry, Technology and Metallurgy, Serbia) and Nadežda Radmilović (Vinca Institute of Nuclear Sciences, Serbia) for help with characterization experiments, as well as the and the National Center for Electron Microscopy, the Molecular Foundry, Lawrence Berkeley National Laboratory, which is supported by the U.S. Department of Energy under Contract # DE-AC02-05CH11231, for the use of electron microscopy and specimen preparation facilities. Authors acknowledge the Ministry of Science, Technological Development and Innovation of the Republic of Serbia (Contract No. 451-03-47/2024-01/200135 and PhD scholarship program) for support.

Conflicts of interest

There are no conflicts to declare.

Data availability

Data presented here can be accessed at the DOI: 10.1039/zenodo.XXXXXX, and it is available under the license CC-BY-4.0 (Creative Commons Attribution-ShareAlike 4.0 International).

Notes and references

1 K. Ellmer, *Nature Photon*, 2012, **6**, 809–817.
2 R. Zhang and M. Engholm, *Nanomaterials*, 2018, **8**, 628.
3 D. S. Ghosh, *Ultrathin Metal Transparent Electrodes for the Optoelectronics Industry*, Springer International Publishing, Heidelberg, 2013.
4 T. Sannicolo, M. Lagrange, A. Cabos, C. Celle, J. Simonato and D. Bellet, *Small*, 2016, **12**, 6052–6075.
5 Z. Wang, Y. Han, L. Yan, C. Gong, J. Kang, H. Zhang, X. Sun, L. Zhang, J. Lin, Q. Luo and C. Ma, *Adv Funct Materials*, 2021, **31**, 2007276.
6 E. Marzbanrad, G. Rivers, P. Peng, B. Zhao and N. Y. Zhou, *Phys. Chem. Chem. Phys.*, 2015, **17**, 315–324.

7 L. M. Vogl, PhD thesis, Friedrich-Alexander-Universität Erlangen-Nürnberg, 2022.
8 D. P. Langley, M. Lagrange, G. Giusti, C. Jiménez, Y. Bréchet, N. D. Nguyen and D. Bellet, *Nanoscale*, 2014, **6**, 13535–13543.
9 J. H. Park, G.-T. Hwang, S. Kim, J. Seo, H.-J. Park, K. Yu, T.-S. Kim and K. J. Lee, *Adv. Mater.*, 2017, **29**, 1603473.
10 B. Hwang, H.-A.-S. Shin, T. Kim, Y.-C. Joo and S. M. Han, *Small*, 2014, **10**, 3397–3404.
11 Y. Liu, J. Zhang, H. Gao, Y. Wang, Q. Liu, S. Huang, C. F. Guo and Z. Ren, *Nano Lett.*, 2017, **17**, 1090–1096.
12 N. Ullah, J. Cui, X. Ren, H. Mei, K. Xu, M. Idrees and X. Mei, *Applied Surface Science*, 2022, **602**, 154343.
13 S. Aghazadehchors, V. H. Nguyen, D. Muñoz-Rojas, C. Jiménez, L. Rapenne, N. D. Nguyen and D. Bellet, *Nanoscale*, 2019, **11**, 19969–19979.
14 V. H. Nguyen, J. Resende, D. T. Papanastasiou, N. Fontanals, C. Jiménez, D. Muñoz-Rojas and D. Bellet, *Nanoscale*, 2019, **11**, 12097–12107.
15 T.-B. Song, Y. S. Rim, F. Liu, B. Bob, S. Ye, Y.-T. Hsieh and Y. Yang, *ACS Appl. Mater. Interfaces*, 2015, **7**, 24601–24607.
16 H. Liu, Y. Li, J. Wu, Y. Fu, H. Tang, X. Yi and Z. Xie, *J. Mater. Chem. C*, 2021, **9**, 9914–9921.
17 L. M. Vogl, V. Kalancha, P. Schweizer, P. Denninger, M. Wu, C. Brabec, K. Forberich and E. Spiecker, *Nanotechnology*, 2023, **34**, 175706.
18 C.-T. Wu, Y.-R. Ho, D.-Z. Huang and J.-J. Huang, *Surface and Coatings Technology*, 2019, **360**, 95–102.
19 A. M. Pourrahimi, D. Liu, V. Ström, M. S. Hedenqvist, R. T. Olsson and U. W. Gedde, *J. Mater. Chem. A*, 2015, **3**, 17190–17200.
20 A. Khan, V. H. Nguyen, D. Muñoz-Rojas, S. Aghazadehchors, C. Jiménez, N. D. Nguyen and D. Bellet, *ACS Appl. Mater. Interfaces*, 2018, **10**, 19208–19217.
21 J.-D. Hwang and Y.-H. Lee, *Phys. Chem. Chem. Phys.*, 2024, 10.1039.D4CP02349H.
22 B. Wei, S. Pan, T. Wang, Z. Tian, G. Chen and T. Xu, *Nanotechnology*, 2016, **27**, 505208.
23 M. Song, J. H. Park, C. S. Kim, D.-H. Kim, Y.-C. Kang, S.-H. Jin, W.-Y. Jin and J.-W. Kang, *Nano Res.*, 2014, **7**, 1370–1379.
24 F. S. F. Morgenstern, D. Kabra, S. Massip, T. J. K. Brenner, P. E. Lyons, J. N. Coleman and R. H. Friend, *Appl. Phys. Lett.*, 2011, **99**, 183307.
25 H. Liu, J. Wu, Y. Fu, B. Wang, Q. Yang, G. D. Sharma, M. L. Keshtov and Z. Xie, *Thin Solid Films*, 2021, **718**, 138486.
26 M. Patel, J. H. Seo, S. Kim, T. T. Nguyen, M. Kumar, J. Yun and J. Kim, *Journal of Power Sources*, 2021, **491**, 229578.
27 Z. Yang, M. Wang, X. Song, G. Yan, Y. Ding and J. Bai, *J. Mater. Chem. C*, 2014, **2**, 4312–4319.
28 S. Mehra, M. G. Christoforo, P. Peumans and A. Salleo, *Nanoscale*, 2013, **5**, 4400.
29 K. Han, M. Xie, L. Zhang, L. Yan, J. Wei, G. Ji, Q. Luo, J. Lin, Y. Hao and C.-Q. Ma, *Solar Energy Materials and Solar Cells*, 2018, **185**, 399–405.
30 D. T. Papanastasiou, A. Sekkat, V. H. Nguyen, C. Jiménez, D. Muñoz-Rojas, F. Bruckert and D. Bellet, *Adv Materials Technologies*, 2023, **8**, 2200563.
31 A.-T. Pham, X.-Q. Nguyen, D.-H. Tran, V. Ngoc Phan, T.-T. Duong and D.-C. Nguyen, *Nanotechnology*, 2016, **27**, 335202.
32 M. Singh, T. R. Rana, S. Kim, K. Kim, J. H. Yun and J. Kim, *ACS Appl. Mater. Interfaces*, 2016, **8**, 12764–12771.
33 W. Lan, Z. Yang, Y. Zhang, Y. Wei, P. Wang, A. Abas, G. Tang, X. Zhang, J. Wang and E. Xie, *Applied Surface Science*, 2018, **433**, 821–828.
34 S. Bai, X. Guo, T. Chen, Y. Zhang and H. Yang, *Thin Solid Films*, 2020, **709**, 138096.
35 Y. Altin, M. Tas, İ. Borazan, A. Demir and A. Bedeloglu, *Surface and Coatings Technology*, 2016, **302**, 75–81.
36 D. Ko, B. Gu, J. Cheon, J.-S. Roh, C. S. Kim, S. Jo, D. C. Hyun and J. Kim, *Materials Chemistry and Physics*, 2019, **223**, 634–640.
37 T. Sannicolo, N. Charvin, L. Flandin, S. Kraus, D. T. Papanastasiou, C. Celle, J.-P. Simonato, D. Muñoz-Rojas, C. Jiménez and D. Bellet, *ACS Nano*, 2018, **12**, 4648–4659.
38 B. Sun and H. Sirringhaus, *Nano Lett.*, 2005, **5**, 2408–2413.
39 R. Yogamalar, R. Srinivasan, A. Vinu, K. Ariga and A. C. Bose, *Solid State Communications*, 2009, **149**, 1919–1923.
40 D. C. Choo and T. W. Kim, *Sci Rep*, 2017, **7**, 1696.
41 H. Oh, J. Lee and M. Lee, *Applied Surface Science*, 2018, **427**, 65–73.
42 P. Guan, R. Zhu, Y. Zhu, F. Chen, T. Wan, Z. Xu, R. Joshi, Z. Han, L. Hu, T. Wu, Y. Lu and D. Chu, *Critical Reviews in Solid State and Materials Sciences*, 2022, **47**, 435–459.
43 S. Koo, J. Park, S. Koo and K. Kim, *J. Phys. Chem. C*, 2021, **125**, 6306–6312.
44 H. G. Manning, F. Niosi, C. G. Da Rocha, A. T. Bellew, C. O'Callaghan, S. Biswas, P. F. Flowers, B. J. Wiley, J. D. Holmes, M. S. Ferreira and J. J. Boland, *Nat Commun*, 2018, **9**, 3219.
45 M. Lagrange, T. Sannicolo, D. Muñoz-Rojas, B. G. Lohan, A. Khan, M. Anikin, C. Jiménez, F. Bruckert, Y. Bréchet and D. Bellet, *Nanotechnology*, 2017, **28**, 055709.
46 S. Lee, J. Jang, T. Park, Y. M. Park, J. S. Park, Y.-K. Kim, H.-K. Lee, E.-C. Jeon, D.-K. Lee, B. Ahn and C.-H. Chung, *ACS Appl. Mater. Interfaces*, 2020, **12**, 6169–6175.
47 B. Stahlmecke, F.-J. Meyer Zu Heringdorf, L. I. Chelaru, M. Horn-von Hoegen, G. Dumpich and K. R. Roos, *Appl. Phys. Lett.*, 2006, **88**, 053122.

Data Availability Statement

The data supporting the findings of this study are available from Zenodo at **10.5281/zenodo.13209287**. Characterization dataset for "Wired for Stability: Evaluating Electrical Performance in Zinc Oxide-Modified Silver Nanowire Solution-Processed Transparent Electrode". Data for main and supporting figures provided as *.xlsx and *.txt files.

For any additional information regarding the data, please contact

Junior researcher, Jovan N. Lukic

Faculty of Technology and Metallurgy

University of Belgrade

Karnegijeva 4, 11120 Belgrade, Serbia

Email: jovlukic@tmf.bg.ac.rs

or

Assistant professor, Vuk Radmilovic

Faculty of Technology and Metallurgy

University of Belgrade

Karnegijeva 4, 11120 Belgrade, Serbia

Email: vukradmilovic@tmf.bg.ac.rs